Inorganic Chemistry
Article

Electrical Conductivity and Spin Crossover: A New Achievement with a Metal Bis Dithiolene Complex

Christophe Faulmann,*,[†] Kane Jacob,[†] Stéphane Dorbes,[†] Stéphane Lampert,[†] Isabelle Malfant,[†] Marie-Liesse Doublet,[‡] Lydie Valade,[†] and José A. Real[§]

Centre National de la Recherche Scientifique, Laboratoire de Chimie de Coordination (LCC/ CNRS/UPR8241), 205, route de Narbonne, 31077 Toulouse (cedex), France, Laboratoire de Structure et Dynamique des Systèmes Moléculaires et Solides USTL II, Place E. Bataillon, 34095 Montpellier cedex 5, France, and Institut de Ciencia Molecular/Departament de Química Inorgànica, Universitat de València, Edificio de Institutos de Paterna, P. B. Box 22085, 46071 Valencia, Spain

Three new compounds based on the cationic complex [Fe^{III}(3-R-salEen)$_2$]$^+$ (salEen stands for *N*-(2-ethylamino)-ethyl)-salicylaldimine, R = H, CH$_3$O) with the electroactive Ni(dmit)$_2$ species as a counterion (dmit stands for 1,3-dithia-2-thione-4,5-dithiolato) have been synthesized and structurally and magnetically characterized. Compound **1** ([Ni(dmit)$_2$][Fe(3-OMe-salEen)$_2$]. CH$_3$OH) shows an apparent hysteresis loop, due to an irreversible desolvatation process. Compound **2** ([Ni(dmit)$_2$](NO$_3$)[Fe(salEen)$_2$]$_2$) exhibits a gradual and incomplete spin transition. Compound **3** ([Ni(dmit)$_2$]$_5$[Fe(salEen)$_2$]$_2$, 6CH$_3$CN) is a fractional oxidation state complex, which behaves like a semiconductor and exhibits a gradual but complete spin transition between 300 and 4 K.

Introduction

There is considerable interest in the synthesis of functional molecule-based materials, not only for fundamental reasons but also for application purposes. This interest resides on the possibility of combining, at will, different components with properties that can be rarely found combined in nature. In favorable cases, it is expected to find some kind of interaction or synergy between each component's property, to generate new functions such as regulation, amplification, phase transition, etc.[1] In this respect, the coordination chemistry of transition-metal ions affords tools, rules, and a rich variety of possibilities to synthesize and explore such new advanced materials. Among them, metal compounds exhibiting switching behavior are among the most interesting components for the construction of such materials. Probably, the most spectacular examples of switchable metal compounds are those undergoing spin crossover (SCO). They may be switched between the low-spin (LS) and high-spin

(HS) states by variation of temperature and/or pressure and by light irradiation.[2–5] LS ↔ HS generally leads to distinctive changes in magnetism, color, and structure, which may induce a strong signal, and a hysteresis is observed in some cases when the molecular structural changes associated with SCO are cooperatively transmitted within the lattice.[6] These singular properties have been investigated in relation with the construction of electronic devices such as memories or sensors, that is, thermal displays,[7] contrast agents for magnetic resonance,[8] as well as the induction of a hysteresis loop in the dielectric constant of SCO compounds.[9]

Nowadays, only a few examples illustrate a combination of SCO properties with other properties in the same solid. For instance, it has been shown that SCO coexists with

---

* To whom correspondence should be addressed. E-mail: faulmann@lcc-toulouse.fr.
[†] Centre National de la Recherche Scientifique.
[‡] Laboratoire de Structure et Dynamique des Systèmes Moléculaires et Solides USTL II.
[§] Institut de Ciencia Molecular/Departament de Química Inorgànica.

(1) Lehn, J.-M. *Science* **2002**, *295*, 2400.
(2) Gütlich, P.; Hauser, A.; Spiering, H. *Angew. Chem., Int. Ed. Engl.* **1994**, *33*, 2024.
(3) Gütlich, P.; Goodwin, H. A. Spin Crossover in Transition Metal Compounds. *Top. Curr. Chem.* **2004**, *233–235*. 2004.
(4) Bousseksou, A.; Molnar, G. *C. R. Chim.* **2003**, *6*, 1175.
(5) Real, J. A.; Gaspar, A. B.; Munoz, M. C. *Dalton Trans.* **2005**, 2062.
(6) Real, J. A.; Gaspar, A. B.; Niel, V.; Munoz, M. C. *Coord. Chem. Rev.* **2003**, *236*, 121.
(7) Kahn, O.; Martinez-Jay, C. *Science* **1998**, *279*, 44.
(8) Muller, R. N.; Vander Elst, L.; Laurent, S. *J. Am. Chem. Soc.* **2003**, *125*, 8405.
(9) Bousseksou, A.; Molnar, G.; Demont, P.; Menegotto, J. *J. Mater. Chem.* **2003**, *13*, 2069.

magnetic exchange,[10] large negative cubic hyperpolarizability,[11] host−guest interactions in porous networks,[12,13] liquid-crystal phase transitions,[14,15] crystalline-state reactions with large structural effects,[16] optical activity of homochiral units,[17] and intermetallic Ag···Ag interactions.[18,19]

Electrical conductivity is a fundamental property of matter currently investigated in the realm of molecular science.[20] The redox active building blocks derived from metal bis-dithiolene complexes display remarkable properties such as conductivity/superconductivity in addition to magnetic and optical properties, which have been investigated in depth.[21] The anionic nature of these complexes makes them good candidates to investigate the coexistence of conductivity and SCO properties in crystalline materials. In this respect, we have chosen to combine the $[Ni(dmit)_2]^{n-}$ complex,[21,22] well-known for its conductive properties when it is present in a fractional oxidation state and the SCO properties of the cationic $[Fe^{III}(L)_x]^+$ complexes, where L represents a Schiff base.

[Ni(dmit)$_2$]$^-$ [Fe(salEen)$_2$]$^+$ [Fe(3-OMesalEen)$_2$]$^+$
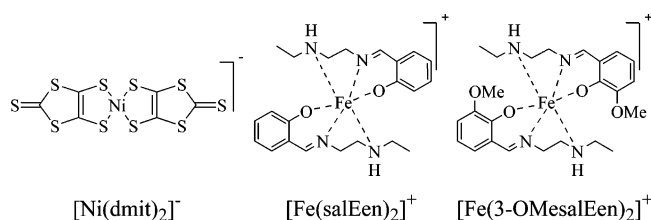
As a first step in this direction, we have recently reported a new SCO compound containing the anionic complex $[Ni(dmit)_2]^-$ (where $dmit^{2-}$ is 2-thioxo-1,3-dithiole-4,5-dithiolato) and the cationic complex $[Fe(sal_2\text{-trien})]^+$.[23] The hexadentate anion $sal_2\text{-trien}^{2-}$ is the doubly deprotonated form of the ligand formed from the condensation of two molecules of salicylaldehyde with triethylenetetramine. This

compound displays strong cooperativity with a wide hysteresis loop, a behavior quite unusual for this family of Fe-(III) complexes,[24] which might be due to the particular arrangement of the crystal packing that favors the occurrence of segregated stacks of cations and anions with a large number of short interactions between them. Recently, Takahashi et al. have published a SCO molecular conductor based on the $[Fe(qsal)_2]^+$ and $[Ni(dmit)_2]^-$ units, namely [Fe-(qsal)$_2$][Ni(dmit)$_2$]$_3$·CH$_3$CN·H$_2$O.[25] These results confirm that the $[Ni(dmit)_2]^-$ unit is indeed a good candidate as a counterion for enhancing cooperativity in SCO complexes based on Fe(III) cations.

In the same line, we have expanded this research to the $[Fe(R\text{-salEen})_2]^+$ cation (R = H or OMe), which is a good candidate in which to observe SCO.[26−28] We report herein the preparation, structure, and the magnetic and electrical properties of three compounds that contain $[Fe(R\text{-salEen})_2]^+$ and $[Ni(dmit)_2]^-$. Two of them are simple 1:1 salts, that is, with the formulas [Ni(dmit)$_2$][Fe(3-OMe-salEen)$_2$], CH$_3$OH (**1**), and [Ni(dmit)$_2$](NO$_3$)[Fe(salEen)$_2$]$_2$ (**2**), and the third one is a fractional oxidation state compound, [Ni(dmit)$_2$]$_5$[Fe-(salEen)$_2$]$_2$, 6CH$_3$CN (**3**).

Experimental Section

General. Syntheses of the starting materials, (NBu$_4$)[Ni(dmit)$_2$], [Fe(salEen)$_2$](NO$_3$), and [Fe(3-OMe-salEen)$_2$](NO$_3$), 0.5H$_2$O were performed by following literature procedures.[27,29]

[Ni(dmit)$_2$][Fe(3-OMe-salEen)$_2$], CH$_3$OH (1) was synthesized by dissolving 151.5 mg (0.266 mmol) of [Fe(3-OMe-salEen)$_2$]-(NO$_3$), 0.5H$_2$O in methanol (50 mL). This solution was sonicated for 1 h and filtered over an acetone solution containing 60.6 mg (0.087 mmol) of (*n*-Bu$_4$N)[Ni(dmit)$_2$]. The resulting precipitate (powder) was filtered, washed with cold acetone, and dried under a vacuum. From the filtrate (maintained at 4 °C overnight), crystals were isolated using a similar procedure as for the powder. Yield: 42 mg (49%). Anal. Calcd for C$_{31}$H$_{38}$FeN$_4$NiO$_5$S$_{10}$: C, 37.92; H, 3.90; N, 5.71; Found powder: C, 38.11; H, 3.50; N, 5.92; crystals: C, 38.22; H, 3.79; N, 5.80.

[Ni(dmit)$_2$](NO$_3$)[Fe(salEen)$_2$]$_2$, CH$_3$CN (2) was synthesized by the addition of an acetonitrile solution (10 mL) of (*n*-Bu$_4$N)-[Ni(dmit)$_2$] (66 mg, 0.095 mmol) over an acetonitrile solution (7 mL) of [Fe(salEen)$_2$)]NO$_3$·H$_2$O (121 mg, 0.242 mmol). The resulting solution was left at 20 °C overnight. After air filtration, dark-green block-like crystals were obtained, washed with acetonitrile, and dried under a vacuum. Yield: 50.7 mg (37%). Anal. Calcd for C$_{52}$H$_{63}$Fe$_2$N$_{10}$NiO$_7$S$_{10}$: C, 43.64; H, 4.44; N, 9.79; Found: C, 44.21; H, 4.48; N, 9.94;

[Ni(dmit)$_2$]$_5$[Fe(salEen)$_2$]$_2$, 6CH$_3$CN (3) was synthesized by the addition of an acetonitrile solution (15 mL) of (*n*-Bu$_4$N)[Ni(dmit)$_2$] (121.2 mg, 0.175 mmol) over an acetonitrile solution (5 mL) of

(10) Real, J. A.; Gaspar, A. B.; Munoz, M. C.; Gütlich, P.; Ksenofontov, V.; Spiering, H. *Top. Curr. Chem.* **2004**, *233*, 167.
(11) Letard, J.-F.; Montant, S.; Guionneau, P.; Martin, P.; Le Calvez, A.; Freysz, E.; Chasseau, D.; Lapouyade, R.; Kahn, O. *Chem. Commun.* **1997**, 745.
(12) Real, J. A.; Andres, E.; Munoz, M. C.; Julve, M.; Granier, T.; Bousseksou, A.; Varret, F. *Science* **1995**, *268*, 265.
(13) Halder, G. J.; Kepert, C. J.; Moubaraki, B.; Murray, K. S.; Cashion, J. D. *Science* **2002**, *298*, 1762.
(14) Fujigaya, T.; Jiang, D.-L.; Aida, T. *J. Am. Chem. Soc.* **2003**, *125*, 14690.
(15) Galyametdinov, Y.; Ksenofontov, V.; Prosvirin, A.; Ovchinnikov, I.; Ivanova, G.; Gütlich, P.; Haase, W. *Angew. Chem., Int. Ed.* **2001**, *40*, 4269.
(16) Niel, V.; Thompson, A. L.; Munoz, M. C.; Galat, A.; Goeta, A. E.; Real, J. A. *Angew. Chem., Int. Ed.* **2003**, *42*, 3760.
(17) Sunatsuki, Y.; Ikuta, Y.; Matsumoto, N.; Ohta, H.; Kojima, M.; Iijima, S.; Hayami, S.; Maeda, Y.; Kaizaki, S.; Dahan, F.; Tuchagues, J.-P. *Angew. Chem., Int. Ed.* **2003**, *42*, 1614.
(18) Galet, A.; Niel, V.; Munoz, M. C.; Real, J. A. *J. Am. Chem. Soc.* **2003**, *125*, 14224.
(19) Niel, V.; Thompson, A. L.; Goeta, A. E.; Enachescu, C.; Hauser, A.; Galet, A.; Munoz, M. C.; Real, J. A. *Chem.—Eur. J.* **2005**, *11*, 2047.
(20) Cassoux, P.; Miller, J. In *Chemistry of Advanced Materials: An Overview*; Interrante, L. V., Hampden-Smith, M. J., Eds.; Wiley-VCH: New York, 1998; pp 19.
(21) Faulmann, C.; Cassoux, P. In *Progress in Inorganic Chemistry*; Stiefel, E. I., Ed.; John Wiley & Sons: New York, 2004; Vol. 52, pp 399−489.
(22) Cassoux, P.; Valade, L. *Inorg. Mater.* **1996**, 1.
(23) Dorbes, S.; Valade, L.; Real, J. A.; Faulmann, C. *Chem. Common.* **2005**, 69.
(24) van Koningsbruggen, P. J.; Maeda, Y.; Oshio, H. *Top. Curr. Chem.* **2004**, *233*, 259.
(25) Takahashi, K.; Cui, H.-B.; Okano, Y.; Kobayashi, H.; Einaga, Y.; Sato, O. *Inorg. Chem.* **2006**, *45*, 5739.
(26) Haddad, M. S.; Lynch, M. W.; Federer, W. D.; Hendrickson, D. N. *Inorg. Chem.* **1981**, *20*, 123.
(27) Haddad, M. S.; Federer, W. D.; Lynch, M. W.; Hendrickson, D. N. *Inorg. Chem.* **1981**, *20*, 131.
(28) Haddad, M. S.; Federer, W. D.; Lynch, M. W.; Hendrickson, D. N. *J. Am. Chem. Soc.* **1980**, *102*, 1468.
(29) Steimecke, G.; Sieler, H. J.; Kirmse, R.; Hoyer, E. *Phosphorus and Sulfur* **1979**, *7*, 49.

Table 1. Crystallographic Data and Experimental Parameters for **1**, **2** and **3**

	1		**2**		**3**	
empirical formula	$C_{31}H_{38}FeN_4NiO_5S_{10}$		$C_{52}H_{63}Fe_2N_{10}NiO_7S_{10}$		$C_{86}H_{78}Fe_2N_{14}Ni_5O_4S_{50}$	
fw	981.81		1431.13		3379.87	
T (K)	293	180	180		293	180
wavelength	0.71069		0.71069		0.71069	
cryst syst	triclinic		monoclinic		triclinic	
space group	$P\bar{1}$		Pn		$P\bar{1}$	
a (Å)	9.9144(17)	9.8749(10)	9.4900(7)		10.1322(9)	10.0392(8)
b (Å)	13.566(3)	13.4501(15)	28.791(3)		11.5857(11)	11.5227(10)
c (Å)	16.205(3)	16.1043(17)	11.9410(9)		30.056(3)	29.915(2)
α (deg)	103.77(2)	103.440(12)	90		82.928(12)	82.625(10)
β (deg)	105.94(2)	105.944(12)	107.224(9)		87.713(12)	87.798(10)
γ (deg)	97.25(2)	97.689(12)	90		66.255(10).	66.151(9)
V (Å³)	1992.2(6)	1955.2(4)	3116.3(4)		3204.8(5)	3138.5(4)
Z	2		2		1	
D_c (g/cm³)	1.637	1.668	1.525		1.751	1.788
μ (mm⁻¹)	1.406	1.432	1.151		1.806	1.844
R_{int}	0.116	0.061	0.030		0.1143	0.1013
reflns collected	11 803	19 473	22 683		24 859	25 366
abs correction	Gaussian		Semiempirical		Gaussian	
data/restraints/params	7238/0/478	7179/0/478	9780/2/904		9553/0/732	9422/0/732
S	0.758	1.061	0.987		0.625	0.893
R1 [$I > 2\sigma(I)$][a]	0.0554	0.0429	0.0235		0.0376	0.0560
wR2 [$I > 2\sigma(I)$][b]	0.0993	0.1083	0.0531		0.0467	0.1257
R1 (all data)	0.1932	0.0707	0.0265		0.1538	0.1148
wR2 (all data)	0.1314	0.1175	0.0540		0.0641	0.1449
absolute structure param			−0.016(7)			
largest diff. peak and hole (e·Å⁻³)	0.613; −0.607	0.741; −0.553	0.210; −0.149		0.378; −0.380	0.810; −0.664

[a] R1 $= \sum||F_o| - |F_c||/\sum|F_o|$. [b] wR2 $= \{\sum[w(F_o^2 - F_c^2)^2]/\sum[w(F_o^2)^2]\}^{1/2}$; $S = \{\sum[w(F_o^2 - F_c^2)^2]/(n - p)\}^{1/2}$, where n is the number of reflections and p is the total number of parameters refined; $w = 1/[\sigma^2(F_o^2) + (aP)^2 + bP]$, with $P = [2F_c^2 + \text{Max}(F_o^2,0)]/3$

[Fe(salEen)$_2$)]NO$_3$·H$_2$O (85.9 mg, 0.175 mmol). The resulting solution was left at 4 °C overnight. After air filtration, dark-green needle-like crystals were obtained, washed with acetonitrile, and dried under a vacuum. Yield: 51.4 mg (43%). Anal. Calcd for $C_{86}H_{78}Fe_2N_{14}Ni_5O_4S_{50}$: C, 30.56; H, 2.33; N, 5.80; Found: C, 31.10; H, 2.42; N, 6.20.

3 can also be obtained by galvanostatic (0.64 μA/cm²) electrochemical oxidation on a platinum anode of a CH$_3$CN solution (16 mL) of **2** (11.9 mg, 0.008 mmol). Needle-like crystals were harvested 7 days later (a few μg).

X-ray Structure Determination. X-ray data were collected at 290 and 180 K for **1** and **3**, and at 180 K for **2**, on a STOE-IPDS diffractometer with monochromatic Mo Kα radiation ($\lambda = 0.71073$ Å). General crystallographic data can be found in Table 1. X-ray structure analysis was performed using the *WinGX* package.[30] In **1** and **3**, hydrogen atoms were included with their calculated positions and riding on their adjacent atom. In **2**, hydrogen atoms belonging to the ethyl groups of the amino nitrogen and those belonging to the acetonitrile molecule were included with their calculated positions and riding on their adjacent atom. Other hydrogen atoms were found by difference Fourier maps and refined (coordinates and isotropic temperature factor). *SIR97*[31] was used for the structure solutions, *Shelxl97*[32] for the refinements, *Platon*[33] for structure analysis and *Ortep3*,[34] *Cameron*,[35] *Mercury*,[36] and *Diamond*[37] for the production of the crystallographic illustrations. Crystallographic

data (excluding structure factors) have been deposited with the Cambridge Crystallographic data Centre as supplementary publication no. CCDC 614048−614052. Copies of the data can be obtained free of charge on application to CCDC, 12 Union Road, Cambridge CB21EZ, U.K. (fax(+44)1223−336-033; E-mail deposit@ccdc.cam.ac.uk).

Measurements of Magnetic Properties. Variable-temperature magnetic susceptibility measurements were performed on powdered samples between 300 and 80 K in a field of 1.5 T, using the Faraday method and using a Quantum Design MPMS2 SQUID susceptometer equipped with a 5.5 T magnet and operating at 1 T and 1.8−375 K. Experimental data were corrected for diamagnetism using Pascal's constants.

Measurements of Electrical Properties. The standard four-probes method was used to measure electrical conductivity on several single crystals. Measurements were performed with ac or dc current. Electrical contacts were made with gold paint on single crystals with an approximate size of ca. 1 × 0.25 × 0.05 mm³. The samples were placed in an Oxford Instruments CF200 continuous flow cryostat for temperature-dependent measurements. Monitoring of the temperature variations and data acquisition were achieved using an Oxford Instruments DTC2/VC30 and a Hewlett-Packard 4263A LCR meter (ac measurements) or a Keithley 2001 multimeter (dc measurements) driven by a PC.

Results and Discussion

The strategy we propose for obtaining conductors based on [Ni(dmit)$_2$]$^{n-}$ and SCO complexes as counterions is to prepare at first a salt of the general formula [Fe(L)][Ni-(dmit)$_2$], by a simple metathesis reaction, and then to oxidize it (chemically or electrochemically) to [Fe(L)][Ni(dmit)$_2$]$_x$

(30) Farrugia, L. J. *J. Appl. Cryst.* **1999**, *32*, 837.
(31) Altomare, A.; Burla, M. C.; Camalli, M.; Cascarano, G. L.; Giacovazzo, C.; Guagliardi, A.; Moliterni, A. G. G.; Polidori, G.; Spagna, R. *J. Appl. Cryst.* **1999**, *32*, 115.
(32) Sheldrick, G. M. *SHELXL97,Programs for Crystal Structure Analysis (Release 97−2)*; University of Göttingen: Göttingen, Germany, 1998.
(33) Spek, A. L. *PLATON, A Multipurpose Crystallographic Tool*; Utrecht University: Utrecht, The Netherlands, 1998.
(34) Farrugia, L. J. *J. Appl. Crystallogr.* **1997**, *30*, 565.
(35) Watkin, D. M.; Pearce, L.; Prout, C. K. *CAMERON-A Molecular Graphics Package*; Chemical Crystallography Laboratory: University of Oxford, 1993.
(36) *Mercury 1.1.2*; Cambridge Crystallographic Data Centre: 12 Union Road. Cambridge. CB2 1EZ. U.K. (http://www.ccdc.cam.ac.uk).
(37) Brandenburg, K. *Diamond 3.1b*, 53002 Bonn, Germany, 2006.

Figure 1. Variation of the $\chi_M T$ product as a function of the temperature for **1** and **1^d** (see text).

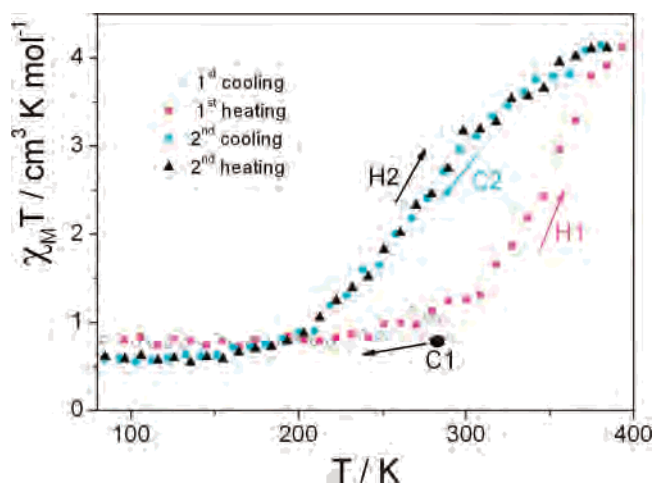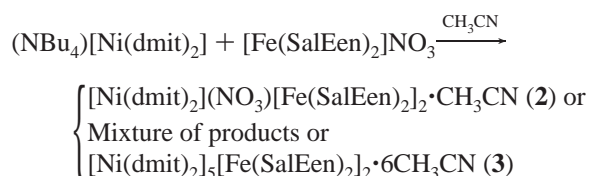**Figure 2.** Variation of the $\chi_M T$ product as a function of the temperature for **2**.

($x > 1$). Therefor our choice for the starting SCO complex has been focused mainly on Fe(III)-based cations rather than on Fe(II)-based cations, to avoid possible oxidation from Fe-(II) to Fe(III) during the electrocrystallization process. To perform good metathesis reactions with the (C)[Ni(dmit)$_2$] salt, solubility properties of the starting SCO complex also determine its choice.

Compound **1** was synthesized by a metathesis reaction from a methanolic solution of [Fe(3-OMe-salEen)$_2$](NO$_3$), 0.5H$_2$O and an acetone solution of (n-Bu$_4$N)[Ni(dmit)$_2$]. Compounds **2** and **3** were synthesized by a metathesis reaction of an acetonitrile solution of [Fe(salEen)$_2$)]NO$_3$·H$_2$O with an acetonitrile solution of (n-Bu$_4$N)[Ni(dmit)$_2$]. Depending on the stoichiometric conditions and the temperature, we have been able to obtain selectively **2** or **3** (Experimental Section).

$$(\text{NBu}_4)[\text{Ni(dmit)}_2] + [\text{Fe(SalEen)}_2]\text{NO}_3 \xrightarrow{\text{CH}_3\text{CN}}$$

$$\left\{ \begin{array}{l} [\text{Ni(dmit)}_2](\text{NO}_3)[\text{Fe(SalEen)}_2]_2 \cdot \text{CH}_3\text{CN (2) or} \\ \text{Mixture of products or} \\ [\text{Ni(dmit)}_2]_5[\text{Fe(SalEen)}_2]_2 \cdot 6\text{CH}_3\text{CN (3)} \end{array} \right.$$

Magnetic Properties. The magnetic data is expressed in the form of $\chi_M T$ versus T for **1**, with χ_M being the molar magnetic susceptibility and T the temperature, is shown in Figure 1. The $\chi_M T$ product is equal to 1.01 cm^3 mol^{-1} K and is almost constant in the temperature range of 80−300 K, indicating that almost all of the Fe^{3+} ions are in the LS state. For temperatures higher than 300 K, $\chi_M T$ increases continuously up to reach a value ca. 4.10 cm^3 mol^{-1} K at 400 K, which is slightly smaller than 4.75 cm^3 mol^{-1} K, the value expected for an uncoupled system of spins $S = ^5/_2 - ^1/_2$, 4.37 cm^3 mol^{-1} K ($g = 2$) for 100% of Fe(III) ions in the HS state plus 0.37 cm^3 mol^{-1} K coming from one unpaired electron associated with the [Ni(dmit)$_2$]$^-$ unit ($g = 2$). It can be estimated that around 15% of the Fe^{3+} complexes are LS at high temperature, whereas only around 4% of the molecules remain HS below 300 K. Consequently, **1** undergoes a rather complete continuous $^5/_2 \leftrightarrow ^1/_2$ spin
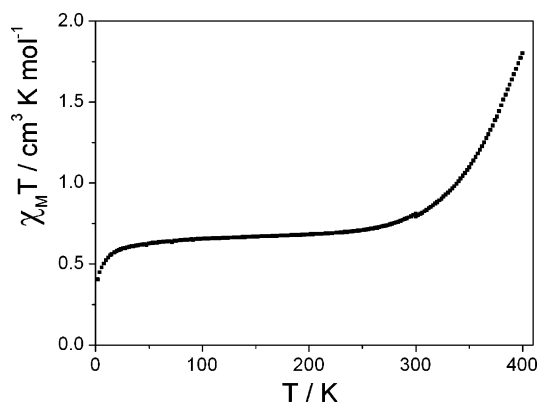
conversion with a characteristic temperature $T_{1/2} = 345$ K (squares in Figure 1). Interestingly, the $\chi_M T$ values in the cooling mode do not match those observed in the heating mode. During this second cooling process, $\chi_M T$ decreases more gradually with $T_{1/2} = 275$ K (filled circles in Figure 1). Below 200 K, $\chi_M T$ reaches a value of 0.65 cm^3 mol^{-1} K, which is constant down to 80 K and consistent with the value expected for an Fe(III) ion in the LS state. Apparently, **1** undergoes a spin transition with a hysteresis loop ca. 70 K wide. To confirm the real nature of this apparent hysteresis, the sample was heated again from 80 K until 400 K was reached. The $\chi_M T$ versus T curve is, within the limit error, identical to that observed when the sample was cooled the first time from 400 K (filled triangles and circles in Figure 1). Such a behavior is commonly observed in SCO compounds when the sample loses solvent molecules. An interesting example was illustrated by Hayami et al. for [Fe-(qsal)$_2$](NCSe)·solvent, (solvent = MeOH, DMSO or CH$_2$-Cl$_2$).[38,39] This fact has been confirmed by DTA-DTG measurements (Supporting Information), which display the loss of one methanol molecule per compound **1** in the temperature interval of 300−400 K. Actually, in Figure 1, the SCO behaviors of two different compounds are displayed: (i) compound **1**, with a gradual spin transition with $T_{1/2} = 345$ K and (ii) its desolvated form **1^d**, with $T_{1/2} = 275$ K.

Attempts to resolvate [Ni(dmit)$_2$][Fe(3-OMe-salEen)$_2$] with methanol failed, as well as attempts to change the nature of the solvent, during the preparation of **1**, by replacing methanol with acetone or acetonitrile. The crystal structure of the desolvated compound could also not be determined, as a result of a lack of crystallinity.

The magnetic behavior of **2** is displayed in Figure 2. At 400 K, $\chi_M T$ (calculated per iron ion) is ca. 1.80 cm^3 K mol^{-1}, which is much below the expected value of 4.75 cm^3 mol^{-1} K for a system containing two noninteracting spin centers, namely one Fe^{3+} ion in the HS state and a formally LS Ni^{3+} ion. Indeed, around 38% of molecules are actually in the

(38) Hayami, S.; Kawahara, T.; Juhasz, G.; Kawamura, K.; Uehashi, K.; Sato, O.; Maeda, Y. *J. Radioanal. Nucl. Chem.* **2003**, *255*, 443.
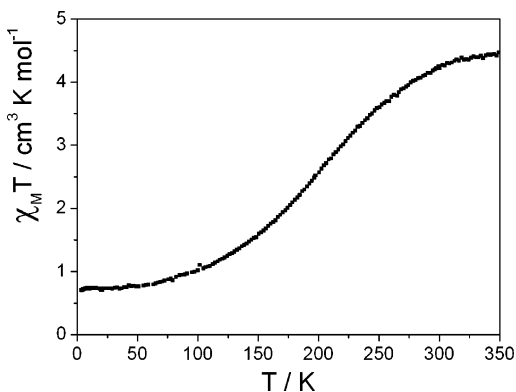(39) Hayami, S.; Gu, Z.-z.; Yoshiki, H.; Fujishima, A.; Sato, O. *J. Am. Chem. Soc.* **2001**, *123*, 11644.

Figure 3. Variation of the $\chi_M T$ product as a function of the temperature for **3**.

Table 2. Selected bond lengths around iron in **1** at 293 and 180 K

distance	293 K		180 K	
Fe−O	1.858(5)	1.869(5)	1.864(3)	1.882(3)
Fe−N(imine)	1.923(6)	1.935(6)	1.922(3)	1.934(3)
Fe−N(amine)	2.057(7)	2.078(6)	2.041(4)	2.052(3)

($S = 1/2$, $g = 2$). Between 300 and 4 K, $\chi_M T$ decreases continuously down to 0.73 cm^3 K mol^{-1}. Cooling and warming modes give identical $\chi_M T$ versus T curves, indicating the occurrence of a practically complete spin transition without a hysteresis and with a characteristic $T_{1/2}$ value of 202 K.

Crystal Structures. [Ni(dmit)$_2$][Fe(3-OMe-salEen)$_2$],-CH$_3$OH (1). The asymmetric unit of compound **1** (Figure 4) consists of one cation [Fe(3-OMe-salEen)$_2$]$^+$, one molecule of methanol, and two halves of Ni(dmit)$_2$ units, with each nickel atom lying on a center of inversion.

The iron atom is in an octahedral environment, with two oxygen, two N$_{amine}$, and two N$_{imine}$ atoms at the corners of the octahedron, and the N$_{imine}$ atoms in the trans position. The tridentate ligands are disposed in a mer configuration. Whatever the temperature, the Fe−O bond distances are the shortest, and the Fe−N$_{amine}$ are the largest (Table 2). No significant changes at 293 and 180 K between the bond lengths are observed, indicating that the iron complex is in the same spin-state (LS), in agreement with the magnetic behavior (Figure 1).

The structure consists of segregated layers of Ni(dmit)$_2$ units and [Fe(3-OMe-salEen)$_2$] cations in the *ab* plane, with CH$_3$OH spreading in between the iron complexes (Figure 5). These layers are interconnected through hydrogen bonds and short intermolecular contacts (shorter than the sum of the van der Waals radii of the involved atoms) (Table S1 in the Supporting Information and Tables 3 and 4) but only between the iron complex and the nickel complex. There also exist such short contacts within each layer (Supporting Information).

In **1**, depending on the temperature, seven to nine short contacts are observed between the solvent molecule and the cation [Fe(3-OMe-salEen)$_2$]$^+$, but no contact is observed between the solvent molecule and the Ni(dmit)$_2$ units. The

HS state at 400 K. Upon cooling down to 300 K, $\chi_M T$ decreases significantly to reach a value of ca. 0.80 cm^3 K mol^{-1}. Then, $\chi_M T$ decreases very slowly from ca. 0.75 to around 0.6 cm^3 K mol^{-1} in the temperature region of 270−25 K. Similar to [Fe(salEen)$_2$](NO$_3$) and [Fe(salEen)$_2$]Cl,[26,40] the [Fe(salEen)$_2$]$^+$cation in **2** is essentially in the LS state, although it displays the onset of a spin conversion between 300 and 400 K. At lower temperatures, the $\chi_M T$ versus T curve decreases more rapidly down to 0.40 cm^3 K mol^{-1} at 5 K. This behavior can be attributed to weak intermolecular antiferromagnetic coupling between two $S = 1/2$ spin carriers. A possible magnetic exchange pathway involves pairs of [Fe-(salEen)$_2$]$^+$ cations connected each other through the NO$_3^-$ anions, which form numerous hydrogen bonds with the cations. In addition, another possible pathway may be the intermolecular contacts observed between the [Fe(salEen)$_2$]$^+$ and the [Ni(dmit)$_2$]$^-$ species (vide infra).

Similar to [Fe(salEen)$_2$](NO$_3$) and [Fe(salEen)$_2$]Cl,[26,40] **2** is essentially in the LS state, although it displays the onset of a spin conversion between 300 and 400 K.

The magnetic behavior of **3** is shown in Figure 3. At 350 K, this compound displays a $\chi_M T$, calculated per iron atom, equal to 4.47 cm^3 K mol^{-1}. As in the case of **1**, this value is slightly smaller than the 4.75 cm^3 K mol^{-1} expected for a system containing one Fe(III) ion in the HS state ($S = 5/2$, $g = 2$) and 2.5 Ni(dmit)$_2$ units sharing a total charge of −1
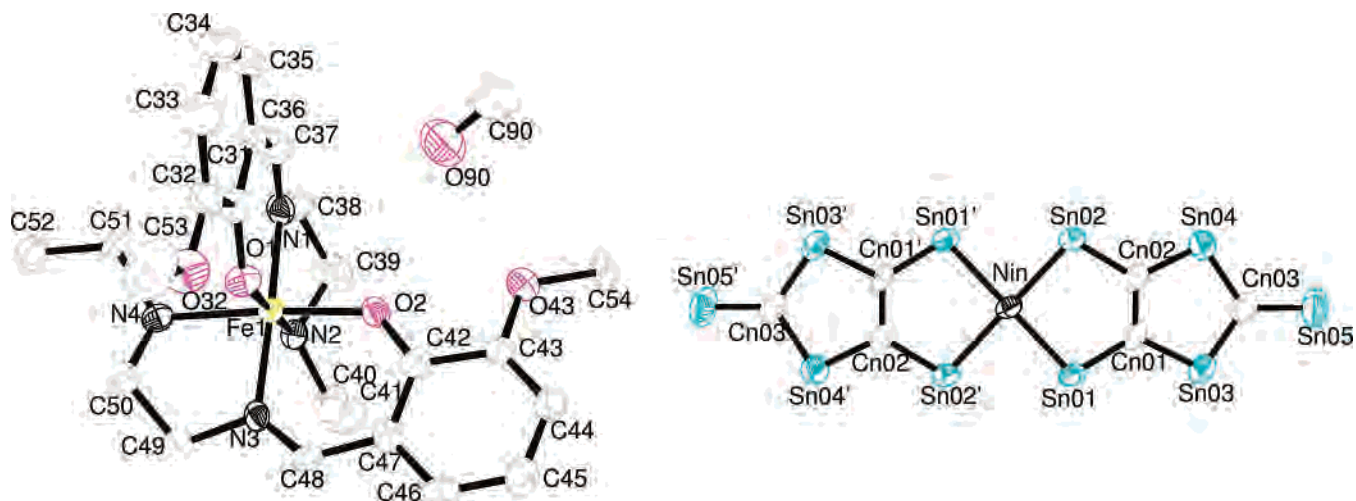

Figure 4. Asymmetric unit of **1** ($n = 1$ or 2) (hydrogen atoms are omitted for clarity reasons).
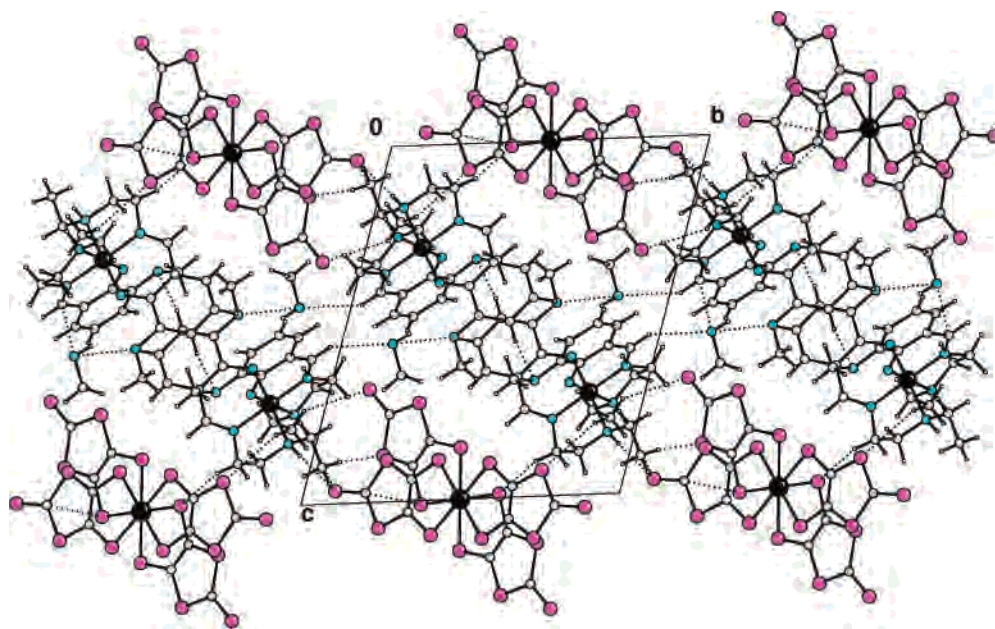
Figure 5. Projection along the *a* axis of the structure of **1** (dotted lines represent short intermolecular contacts).

Table 3. Hydrogen bonds in **1**

				distance (Å)			angle (deg)
D−H	A	Symmetry operation to be applied on atom A	*T* (K)	D−H	H···A	D···A	D−H···A
N(2)−H(2)	S(205)	*x*, −1 + *y*, *z*	290	0.91	2.77	3.671(7)	169
			180	0.93	2.74	3.662(3)	170
N(4)−H(4)	S(205)	*x*, −1 + *y*, *z*	290	0.91	2.64	3.540(7)	173
			180	0.93	2.60	3.520(4)	172
O(90)−H(90)	O(43)	−1 + *x*, *y*, *z*	290	0.82	2.21	2.96(1)	152
			180	0.84	2.23	2.934(5)	145
O(90)−H(90)	O(2)	−1 + *x*, *y*, *z*	180	0.84	2.47	3.227(4)	148
C(52)−H(52B)	S(103)	1 + *x*, −1 + *y*, *z*	180	0.98	2.87	3.832(5)	166

Table 4. Selected Short Intermolecular Contacts (Shorter than the Sum of the van der Waals Radii of the Involved Atoms) between $[Fe(3\text{-OMe-salEen})_2]^+$ and MeOH in **1**

		Distance (Å) atom 1···atom 2	
atom 1	atom 2[a]	at 290 K	and 160 K
C54	H90C	2.718	2.726
C37	O90	3.021	3.011
H54B	H90C	2.357	2.350
O43	H90C	2.682	2.669
O2	H90	2.701	2.483
O43	O90	2.960	2.934
O43	H90	2.214	2.206
O90	H37*		2.630
H37	O90*		2.630

[a] Symmetry operation to be applied on atom 2: −*x*, −*y*, 1 − *z*.

loss of methanol during the first spin transition (H1 in Figure 1) results in the loss of these short contacts in the subsequent cooling and heating processes (C2 and H2 in Figure 1). Moreover, this loss of solvent might also be at the origin of slight changes in the structural packing of the cations, which probably do not exhibit the same interaction network, before and after desolvation. Unfortunately, the lack of structural data after desolvation does not claim this without ambiguity. Nevertheless, the analysis of the short contacts network at 160 and 290 K clearly shows there are more contacts and shorter at 160 K (47) than at 290 K (33). The schematic

view of the structure excluding the solvent (Figure 6) clearly shows that that the iron complexes are much more isolated within their layer than in the solvated compound. This arrangement leads to a less efficient cooperativity than in the solvated compound, in agreement with the broad spin transition observed during C2 and H2 (Figure 1).

$[Ni(dmit)_2](NO_3)[Fe(salEen)_2]_2 \cdot CH_3CN$ **(2).** Compound **2** consists of two cations $[Fe(salEen)_2]^+$, one $[Ni(dmit)_2]^-$, one counterion $(NO_3)^-$, and one CH_3CN molecule (Figure 7).

In both cations, the iron atom is in an octahedral environment, with two oxygen, two N_{amine}, and two N_{imine} atoms at the corners of the octahedron, and the two ligands in a mer configuration. As in **1**, the Fe−O bond distances are the shortest (averaged distance 1.87 Å), whereas the Fe−N_{amine} distances are the largest (averaged 2.04 Å) (Table 5). The environment around iron is identical in both cations: indeed no discrepancy is observed between bond distances and related bonds angles (Table 5). One can then deduce that both cations are in the same spin state. The iron atom is in an almost regular octahedral environment, as shown by the small discrepancies within the values of the bond lengths (close to 1.90 Å) and bond angles (close to 90 or 180 °).

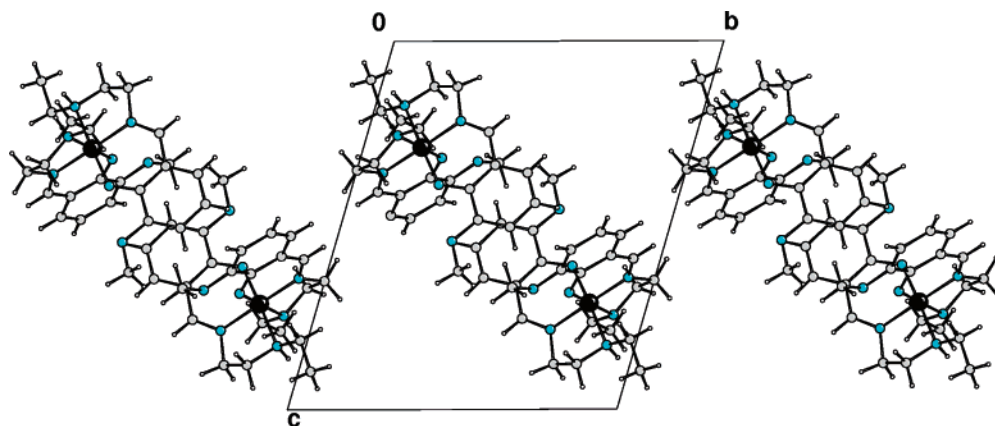(40) Field, C. N.; Boillot, M.-l.; Clement, R. *J. Mater. Chem.* **1998**, *8*, 283.

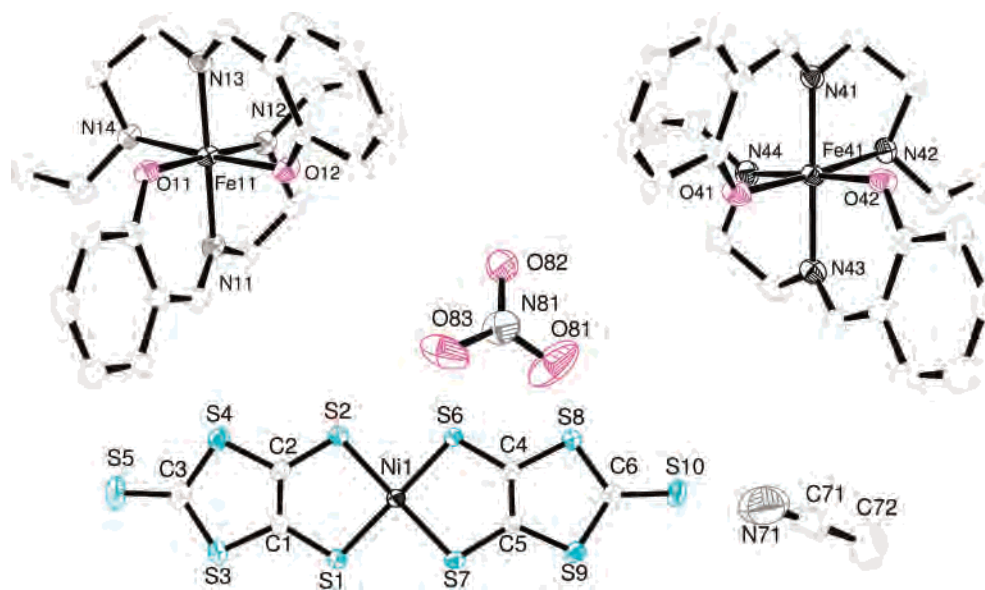**Figure 6.** Structure of **1** without the methanol molecule.

Figure 7. Asymmetric unit of **2** (hydrogen atoms are omitted for clarity reasons).

Table 5. Selected Bond Lengths and Bond Angles around iron in **2**

distance	cation 1		cation 2	
Fe–O	1.868(2)	1.873(2)	1.867(2)	1.871(2)
Fe–N(imine)	1.921(2)	1.925(2)	1.928(2)	1.929(2)
Fe–N(amine)	2.037(2)	2.047(2)	2.036(2)	2.041(2)
angle	cation 1		cation 2	
O–Fe–O	93.16(8)		94.20(8)	
O–Fe–N(imine)	84.88(9)	86.95(8)	85.98(9)	84.84(9)
O–Fe–N(imine)	92.98(9)	93.99(9)	92.65(9)	93.56(9)
N(imine)–Fe–N(imine)	178.86(10)		177.82(10)	
O–Fe–N(amine)	88.71(9)	88.63(10)	88.24(9)	87.69(9)
O–Fe–N(amine)	176.41(10)	175.95(10)	177.62(9)	175.90(9)
N(imine)–Fe–N(amine)	95.99(9)	97.95(9)	96.97(9)	97.55(10)
N(imine)–Fe–N(amine)	84.13(9)	83.73(10)	84.16(9)	83.89(9)
N(amine)–Fe–N(amine)	90.00(10)		89.68(10)	

At 180 K, in **2**, the $[Fe(salEen)_2]^+$ cations form zigzag layers in the *ac* plane. Because there are two iron complexes in the asymmetric unit, they are not equivalent. Therefor, acetonitrile molecules are intercalated only between the Fe11 complexes. These iron layers are separated from each other along the *b* direction by layers of $[Ni(dmit)_2]^-$ and $(NO_3)^-$ anions (Figure 8). The two layers are connected to each other (i) through hydrogen bonds between the hydrogen of the nitrogen(amino) atoms of the iron units and the nitrate anion

(Table 6) and (ii) through short intermolecular contacts (shorter than the sum of the Van der Waals radii of concerned atoms).

The $Ni(dmit)_2$ unit is not planar, because the two Nidmit parts form an angle of $14.91(4)°$, indicating that the nickel atom is in a distorted square-planar environment (Figure 9), which is not uncommon for $[Ni(dmit)_2]^-$ complexes.[41–46]

$[Ni(dmit)_2]_5[Fe(salEen)_2]_2, 6CH_3CN$ (3). The asymmetric unit of **3** consists of one cation $[Fe(salEen)_2]^+$, two $Ni(dmit)_2$ moieties, one-half $Ni(dmit)_2$ moiety (with nickel on a center of inversion), and three acetonitrile molecules (Figure 10). Every cell parameter, with the exception of *c*, decreases when the temperature is lowered from 290 to 180 K. This

(41) Faulmann, C.; Veldhuizen, Y. S. J.; Haasnoot, J. G.; Reedijk, J.; Cassoux, P. *Acta Crystallogr., Sect. C* **1998**, *C54*, 1827.
(42) Nishihara, S.; Akutagawa, T.; Hasegawa, T.; Nakamura, T. *Inorg. Chem.* **2003**, *42*, 2480.
(43) Akutagawa, T.; Takamatsu, N.; Kozo, Shitagami, T. H.; Nakamura, T.; Inabe, T.; Fujita, W.; Awaga, K. *J. Mater. Chem.* **2001**, *11*, 2118.
(44) Hirose, T.; Imai, H.; Naito, T.; Inabe, T. *J. Solid State Chem.* **2002**, *168*, 535–546.
(45) Tomono, K.; Sasaki, Y.; Miyamura, K. *Acta Cryst.* **2005**, *E61*, m18.
(46) Qi, F.; Xiao-Zeng, Y.; Jin-Hua, C.; Mei-Yun, H. *Acta Cryst., Sect. C* **1993**, *49*, 1347.
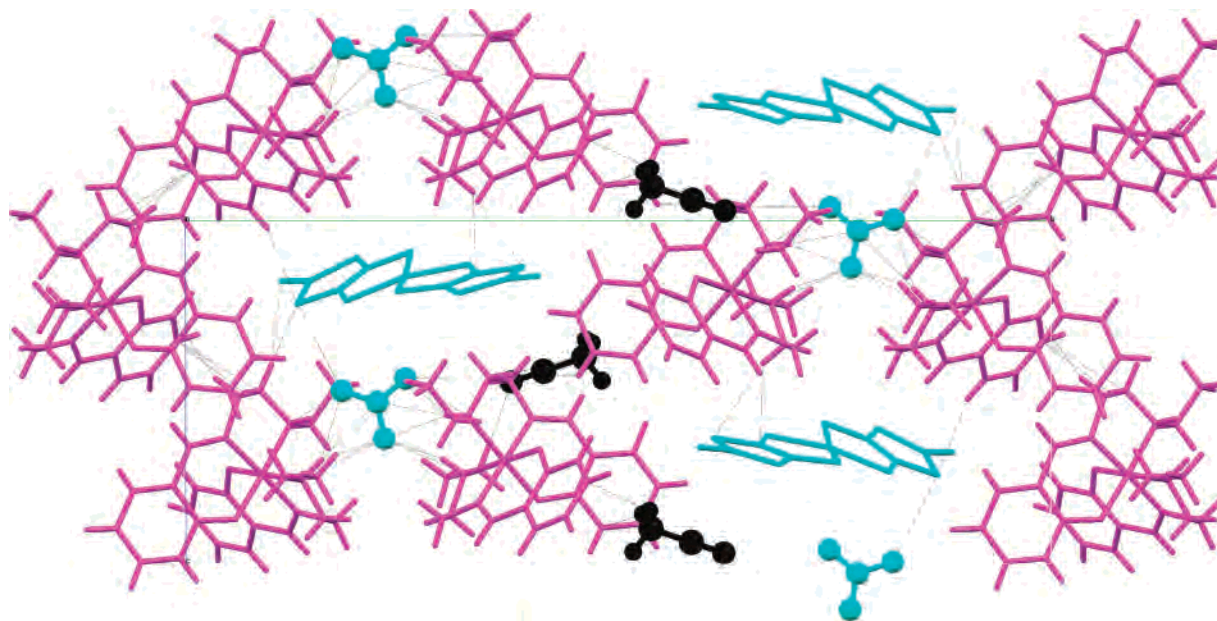
Figure 8. Projection along the *a* axis of the structure of **2** (acetonitrile and nitrate are shown in black and cyan (or light gray) sticks and balls, respectively; dotted lines represent short intermolecular contacts).

Figure 9. Side view of the Ni(dmit)$_2$ moiety in **2**.

Table 6. Hydrogen bonds between the Anionic and Cationic Layers in **2**

D−H···A	distance (Å)			angle (deg)
	D···H	H···A	D···A	D−H···A
N12−H12N···O82	0.88(3)	2.11(3)	2.960(3)	164(2)
N14−H14N···O81	0.84(3)	2.27(3)	3.005(5)	147(2)
N14−H14N···O82	0.84(3)	2.51(3)	3.319(4)	161(2)
N42−H42N···O83	0.82(3)	2.14(3)	2.915(4)	159(3)
N44−H44N···O82	0.92(3)	2.21(3)	3.054(3)	153(3)
N44−H44N···O83	0.92(3)	2.41(3)	3.242(3)	152(3)

induces a cell volume diminution of ca. 2.07%. The coordination environment of iron atoms is identical to that observed in **2**: two N$_{amine}$ (N2, N4), two N$_{imine}$ (N1, N3), and two oxygen atoms are at the corner of the octahedron centered on the iron atom.

As in **2**, the Fe−O bond distances are the shortest and the Fe−N$_{amine}$ distances are the largest (Table 7). When decreasing the temperature, the Fe−O bond lengths do not change significantly, whereas the Fe−N$_{imine}$ bond lengths decrease ca. 2.4% (1.98 Å at 290 K and 1.93 Å at 180 K), and the Fe−N$_{amine}$ bond lengths decrease ca. 3.4% (2.11 Å at 290 and 2.04 Å at 180 K) (Table 7).

When the temperature decreases, the angle N$_{imine}$−Fe−N$_{imine}$ tends to become more linear (Table 7). This is also observed for the angles O−Fe−N$_{amine}$. Even if some angles tend to differ from 90° at 180 K, the combination of these variations in bond lengths and bond angles results in a more regular octahedral environment at 180 K than at 290 K (Figure 11). This is further evidenced by a less-distorted equatorial plane (O1O2FeN2N4: max. deviations: 0.12 Å at 290 K and 0.05 Å at 180 K). The values reported in Table 7 indicate that the Fe(salEen)$_2$ cations are mainly in the LS

Table 7. Bond Lengths and Angles around iron in **3**

distances (Å)	290 K	180 K	angles (°)	290 K	180 K
Fe−O	1.879(6)	1.870(5)	O−Fe−O	94.7(2)	94.1(2)
	1.885(5)	1.886(6)			
Fe−N$_{imine}$	1.983(6)	1.932(6)	O−Fe−N$_{imine}$	90.2(2)	93.2(2)
	1.984(7)	1.939(6)		90.9(2)	93.2(3)
				91.3(3)	86.8(3)
				91.1(2)	86.8(2)
Fe−N$_{amine}$	2.114(5)	2.042(7)	N$_{imine}$−Fe−N$_{imine}$	177.5(2)	179.9(3)
	2.114(6)	2.044(7)			
			O−Fe−N$_{amine}$	88.2(2)	84.7(3)
				87.6(2)	86.9(3)
				172.7(3)	176.5(2)
				173.0(3)	177.3(3)
			N$_{amine}$−Fe−N$_{amine}$	90.3(2)	91.5(3)

Table 8. Hydrogen Bonds within the Cationic Layer and Hydrogen Bonds within **3**

D−H···A		D···H (Å)	H···A (Å)	D···A (Å)	Angle (deg) D−H···A
N(2)−H(2)···N(301)	290 K	0.91	2.35	3.118(11)	142
	180 K	0.93	2.27	3.066(11)	143
N(4)−H(4)···N(301)	290 K	0.91	2.48	3.296(14)	149
	180 K	0.93	2.46	3.288(13)	149

state at 180 K and in the HS state at 290 K. This is in agreement with what is observed in the magnetic measurements (Figure 3).

At 290 and 180 K, in **3**, the [Fe(salEen)$_2$]$^+$ cations and the solvent molecules form double layers in the *ab* plane. These double layers are separated from each other along the *c* direction by layers of [Ni(dmit)$_2$]$^-$ (Figure 12).

Within the cationic layer, the [Fe(salEen)$_2$]$^+$ cations and the solvent molecules are connected to each other on the one hand through two hydrogen bonds between the amino hydrogens and the nitrile groups of one solvent molecule (Figure 12, Table 8 and Figure S1 in the Supporting Information) and on the other hand through a network of short contacts (shorter than the sum of the Van der Waals
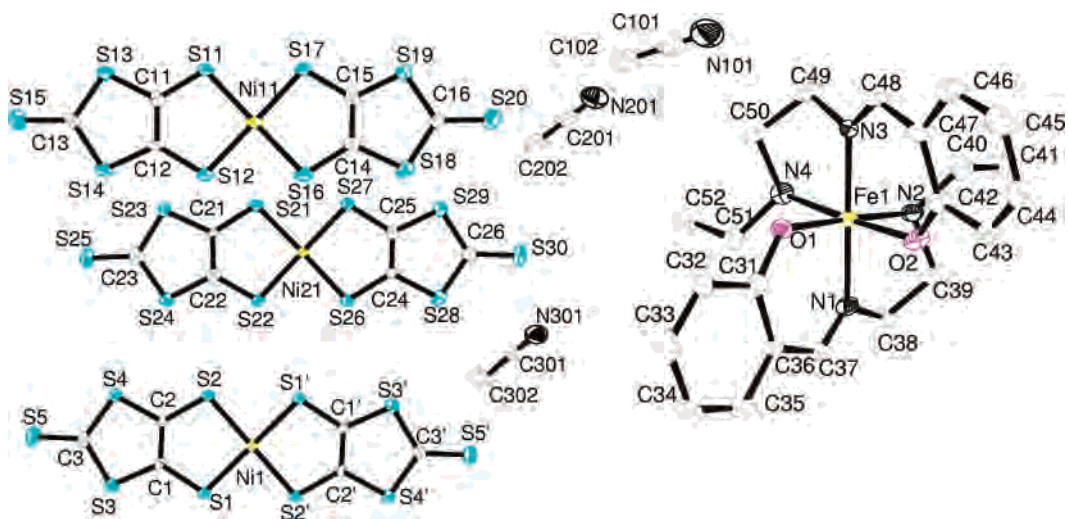
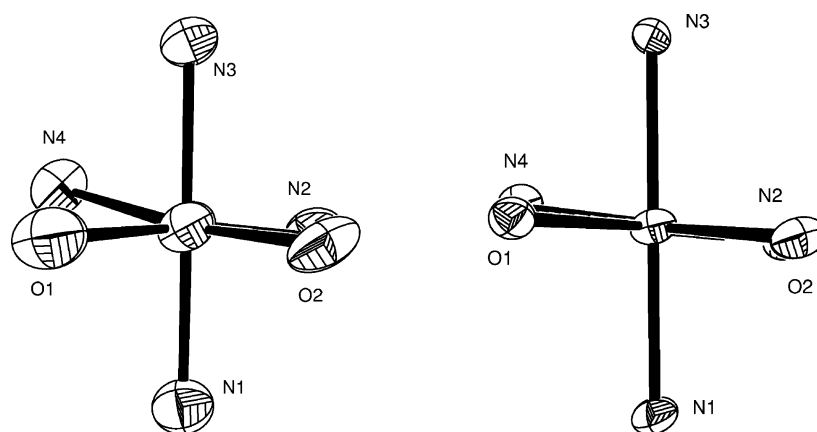**Figure 10.** Asymmetric unit of **3**.

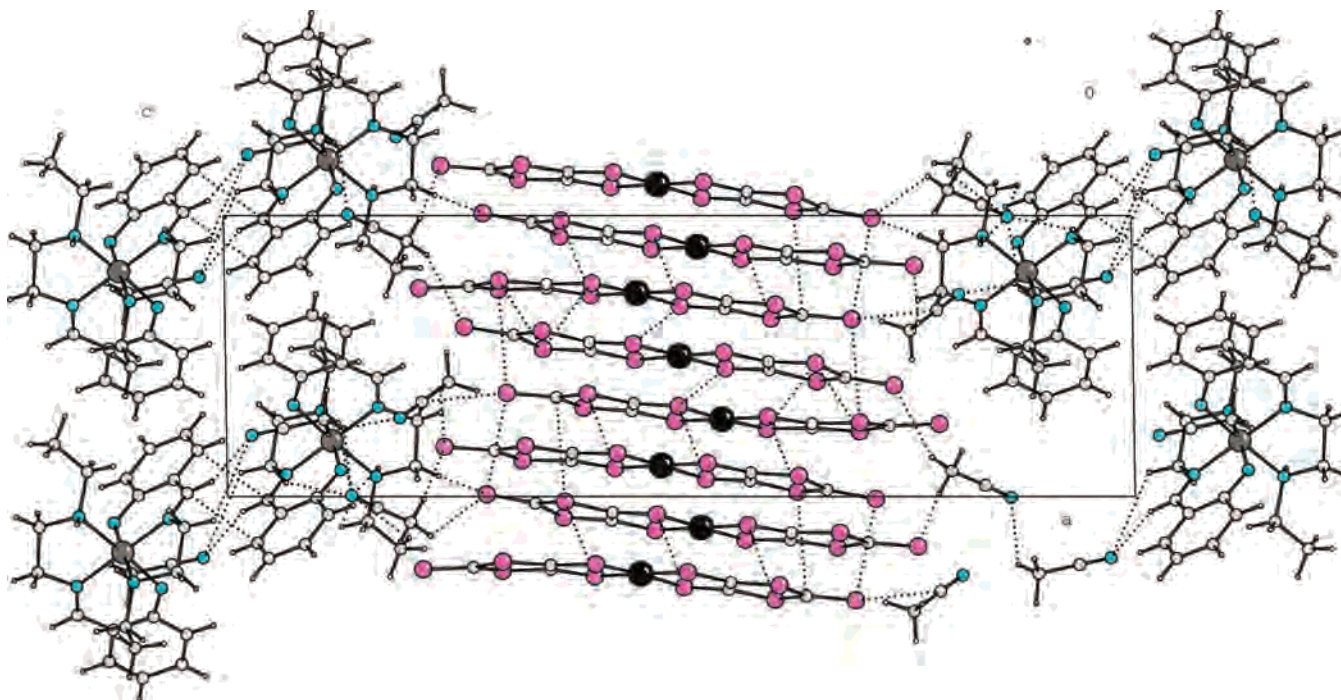**Figure 11.** Octahedral environment of iron in **3** at 290 (left) and 180 K (right).

Figure 12. Projection of the structure of **3** at 180 K along *a* (right) and along *b* (left) (dotted lines represent short intermolecular contacts).
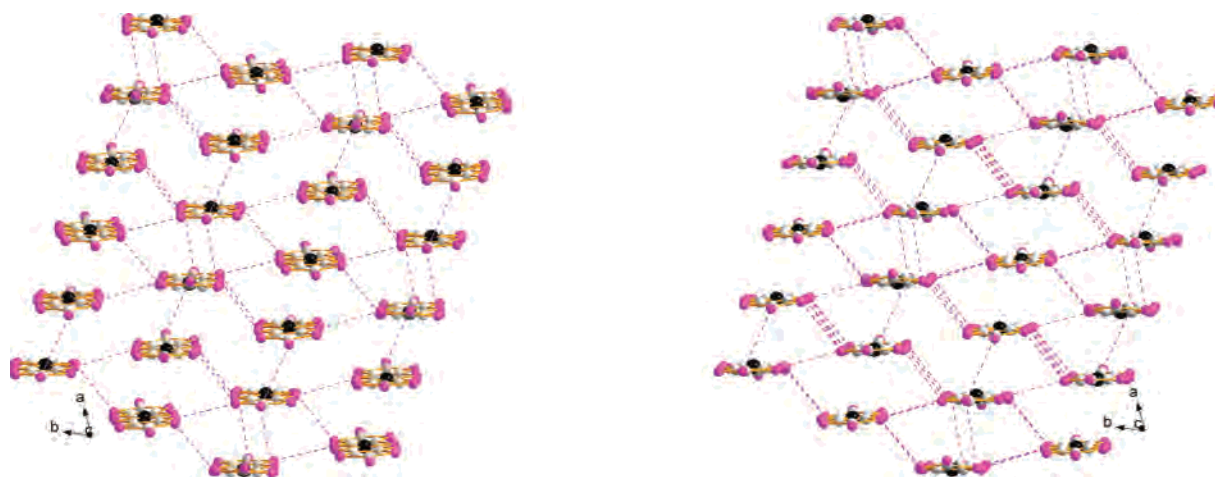
Figure 13. Stacks of the Ni(dmit)$_2$ units in **3** viewed along their long axis at 290 K (left) and at 180 K (right).

Table 9. Short Intermolecular Contacts (< sum of van der Waals Radii) within the Cationic Layer in **3**

	atom 1	atom 2	symmetry operation to be applied on atom 2	distance (Å) 290 K	distance (Å) 180 K
[Fe]−[Fe]	C35	C37	$-x, 1-y, -z$	3.320	3.232
	C37	C35	$-x, 1-y, -z$	3.320	3.232
[Fe]−solvent	C32	H10B	x, y, z	2.755	2.751
	C45	H10C	x, y, z	2.813	2.785
	C46	H10C	x, y, z	2.773	2.731
	H37	N101	$-x, 1-y, -z$	2.691	2.663
	H4	N201	$-1+x, 1+y, z$	2.730	2.675
	H38B	N201	$-1+x, 1+y, z$	2.746	2.699
	H2	N301	x, y, z	2.351	2.272
	H4	N301	x, y, z	2.484	2.459
	H49A	N301	x, y, z	2.605	2.583
	N101	H37	$-x, 1-y, -z$	2.691	2.663
	N201	H4	$1+x, -1+y, z$	2.730	2.675
	N201	H38B	$1+x, -1+y, z$	2.746	2.699
	N101	H39A	$x, -1+y, z$	2.733	
	H52C	C201	$-1+x, 1+y, z$	2.893	
	H39A	N101	$x, 1+y, z$	2.733	
	N2	N301	x, y, z		3.066
	C201	H52C	$1+x, -1+y, z$	2.893	
solvent−solvent	N201	N301	$1+x, -1+y, z$	3.098	3.077
	N301	N201	$-1+x, 1+y, z$	3.098	3.077

radii of concerned atoms) (Table 9). It should be pointed out that there are only two direct contacts between the iron complexes, whatever the temperature (Table 9). When the temperature decreases, the length of these interactions also decreases. However, at 180 K, less contacts are observed between [Fe(salEen)$_2$]$^+$ and the solvent than at 290 K. This might be due to the difference in the volume of the cation at 290 and 180 K. This poor network of interactions might explain the weak cooperativity of **3**, which exhibits a gradual spin transition (Figure 3).

The cationic layer is connected to the anionic layer through many short contacts (shorter than the sum of the van der Waals radii) (Figure 12, Table 10). When the temperature decreases, the number of these interactions increases significantly (10 contacts at 290 K to be compared to 15 contacts at 180 K), and the length of these interactions decreases.

Within the anionic layer, the Ni(dmit)$_2$ units are connected through an important 2D network of S···S contacts (Figure 13), ranging from 3.43 to 3.60 Å (Table 11). These contacts are largely dependent on the temperature because they are shorter and their number is two times larger at 180 than at 290 K.

Electrical Properties. The electrical conductivity of **3** is ca. 0.12 S.cm^{-1} at 295 K (Figure 14). The conductivity decreases at 100 K ($\sigma = 1 \ 10^{-4}$ S.cm^{-1}) with a semiconducting behavior ($E_a = 80$ meV). Below 100 K, the compound

Table 10. Short Contacts Between the Cationic and the Anionic Layers in **3**

	atom 1	atom 2	symmetry operation to be applied on atom 1 and on atom 2		distance (Å) 290 K	distance (Å) 180 K
[Ni]−[Fe]	H50A	S20	x, y, z	x, y, z	2.971	2.941
	H50B	S15	x, y, z	$-x, 1-y, 1-z$	2.938	2.872
	S15	H50B	x, y, z	$-x, 1-y, 1-z$	2.938	2.872
	H49B	S20	x, y, z	x, y, z		2.978
	S25	C301	x, y, z	$1-x, 1-y, 1-z$		3.475
	C301	S25	x, y, z	$1-x, 1-y, 1-z$		3.475
[Ni]−solvent	S20	H20C	x, y, z	$-1+x, y, z$	2.903	2.878
	H20A	S5	x, y, z	$1-x, 1-y, 1-z$	2.974	2.846
	H20C	S20	x, y, z	$1+x, y, z$	2.903	2.878
	S5	H20A	$1-x, 2-y, 1-z$	$x, 1+y, z$	2.974	2.846
	S5	H20A	x, y, z	$1-x, 1-y, 1-z$	2.974	2.846
	S25	H30B	x, y, z	$1-x, 1-y, 1-z$	2.996	
	H30B	S25	x, y, z	$1-x, 1-y, 1-z$	2.996	
	S15	H20A	x, y, z	$1-x, -y, 1-z$		2.983
	S20	H30C	x, y, z	$x, -1+y, z$		2.948
	H20A	S15	x, y, z	$1-x, -y, 1-z$		2.983
	H30C	S20	x, y, z	$x, 1+y, z$		2.948

Figure 14. Electrical conductivity of **3** as a function of the temperature.

Table 11. Short Intermolecular S···S Contacts between [Ni(dmit)$_2$] in **3**

atom 1	atom 2	symmetry operation to be applied on atom 1	and on atom 2	distance (Å) at 290 K	at 180 K
S4	S27	$1-x, 2-y, 1-z$	$x, 1+y, z$	3.558	3.521
S4	S27	x, y, z	$1-x, 1-y, 1-z$	3.558	3.521
S2	S24	$1-x, 2-y, 1-z$	$1-x, 2-y, 1-z$	3.551	3.509
S15	S25	x, y, z	$-1+x, y, z$	3.582	3.530
S11	S21	x, y, z	$1-x, -y, 1-z$	3.544	3.503
S12	S22	x, y, z	$1-x, 1-y, 1-z$	3.464	3.434
S16	S24	x, y, z	$1-x, 1-y, 1-z$	3.532	3.493
S27	S4	x, y, z	$1-x, 1-y, 1-z$	3.558	3.521
S25	S28	x, y, z	$1-x, 1-y, 1-z$	3.556	3.532
S28	S25	x, y, z	$1-x, 1-y, 1-z$	3.556	3.532
S25	S15	x, y, z	$1+x, y, z$	3.582	3.530
S21	S11	x, y, z	$1-x, -y, 1-z$	3.544	3.503
S22	S12	x, y, z	$1-x, 1-y, 1-z$	3.464	3.434
S24	S16	x, y, z	$1-x, 1-y, 1-z$	3.532	3.493
S2	S24	x, y, z	x, y, z	3.551	3.509
S2	S22	x, y, z	x, y, z		3.589
S1	S22	$1-x, 2-y, 1-z$	x, y, z		3.594
S4	S29	$1-x, 2-y, 1-z$	$x, 1+y, z$		3.584
S4	S29	x, y, z	$1-x, 1-y, 1-z$		3.584
S1	S22	x, y, z	$1-x, 2-y, 1-z$		3.594
S2	S22	$1-x, 2-y, 1-z$	$1-x, 2-y, 1-z$		3.589
S11	S11	x, y, z	$-x, -y, 1-z$		3.591
S11	S17	x, y, z	$-x, -y, 1-z$		3.582
S13	S17	x, y, z	$-x, -y, 1-z$		3.595
S13	S19	x, y, z	$-x, -y, 1-z$		3.593
S17	S11	x, y, z	$-x, -y, 1-z$		3.582
S17	S13	x, y, z	$-x, -y, 1-z$		3.595
S19	S13	x, y, z	$-x, -y, 1-z$		3.593
S14	S26	x, y, z	$1-x, 1-y, 1-z$		3.594
S29	S4	x, y, z	$1-x, 1-y, 1-z$		3.584
S26	S14	x, y, z	$1-x, 1-y, 1-z$		3.594

does not behave like a pure resistance, but like an impedance with a strong out-of-phase signal, giving unreliable resistance values. This behavior is totally reversible.

This electrical behavior is deceiving with regard to the crystal structure and the fractional oxidation state of [Fe-(salEen)$_2$]$_2$[Ni(dmit)$_2$]$_5$·6CH$_3$CN. This semiconducting behavior when the temperature decreases seems to act in an opposite manner than the increasing number of S···S contacts between 290 and 100 K. Actually, the larger number of contacts is mainly due to supplementary contacts between adjacent stacks, but not within a stack. Their efficiency may therefor be rather limited (vide infra).

Electronic Structure. Extended Hückel tight-binding (EHTB) calculations have been performed for the two anionic structures refined at 290 and 180 K, using the *CAESAR* code.[47] They reveal that the Ni(dmit)$_2$ slabs are better represented by a weakly interacting pentamer, [Ni(dmit)$_2$]$_5^{2-}$ units (Figure 15), as depicted by the intra- (A,B) and inter-pentamer (C−H) interactions energies listed in Table 12. Within a column, these pentamer units are even more disconnected from each other when the temperature decreases, as shown by the interaction energies calculated for the $T = 180$ K structure: A and B (intra-pentamer interac-

tions) increase, whereas I (inter-pentamer interaction) decreases. Simultaneously, most interactions with adjacent columns also decrease (with the exception of D). Globally, this reinforces the pentameric character of the Ni(dmit)$_2$ slabs. As a consequence, the two electrons carried by the anionic part are mainly localized on the five [Ni(dmit)$_2$] units, as
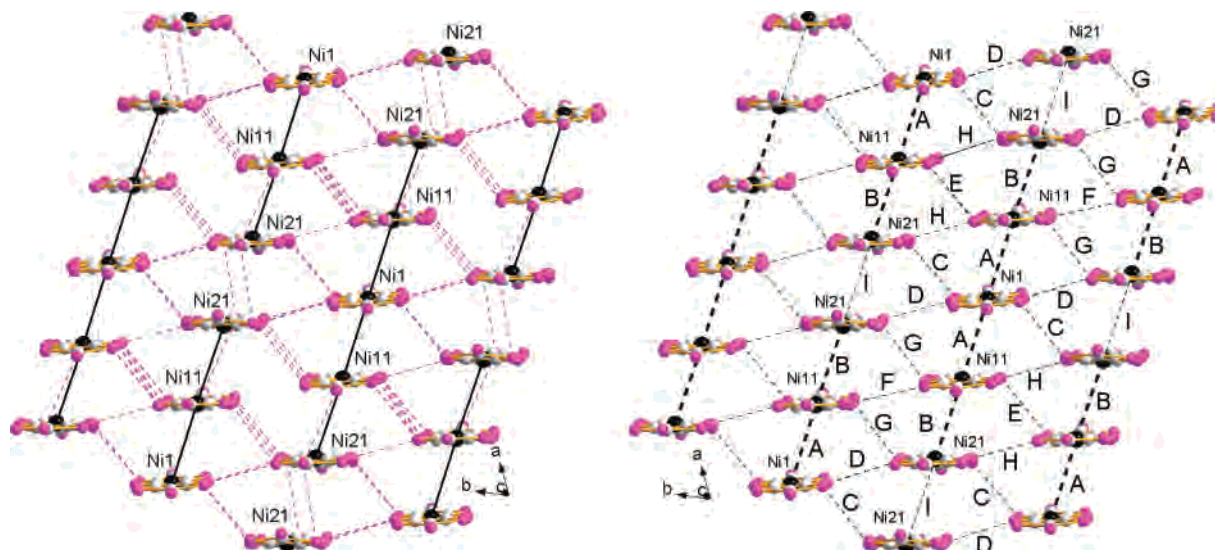
Figure 15. View of the [Ni(dmit)$_2$] slab showing the pentamerization (left) and their interaction according to Table 12.

Table 12. Interaction Energies β(eV) Calculated with the EHTB Method for the Different Ni(dmit)$_2$···Ni(dmit)$_2$ Interactions in the Ni(dmit)$_2$ Slabs[a]

	$T = 290$ K	$T = 180$ K	
Type	β (eV)		Variation in %
A	0.2929	0.3171	+8.3
B	0.2698	0.2963	+9.8
I	0.0409	0.0353	−13.7
C	0.0209	0.0217	+3.8
D	0.0088	0.0106	+20.5
E	0.0614	0.0569	−7.3
F	0.0096	0.0088	−8.33
G	0.0054	0.0022	−59.2
H	0.0002	0.0002	0

[a] The preparation and characterization of metal bisdithiolene compounds exhibiting spin transition (and electrical properties in one compound) are reported. These compounds are based on the [Ni(dmit)$_2$]$^-$ anion and the [Fe(R-salEen)$_2$]$^+$ cations (R = H and OMe).

supported by the very small dispersions calculated for the five LUMO bands of the Ni(dmit)$_2$ slab (Figure 16). In agreement with the semiconducting behavior of this phase, a small gap is observed around X(1/2,0) in the room-temperature electronic band structure, which increases when the temperature decreases (see Supporting Information for the low-temperature electronic band structure).

Conclusions

Three new compounds based on Ni(dmit)$_2$ with a SCO unit as a counterion have been obtained. Such an association was envisioned for combining in the same compound electrical and magnetic properties. **1** and **2** are not in a fractional oxidation state, and therefor do not exhibit any electrical properties. Nevertheless, both exhibit a spin transition. Actually, as already observed for analogous compounds derived from the Ni(dmit)$_2$ units,[23] substituting the innocent nitrate anion in the reactant [Fe(3-R-salEen)$_2$](NO$_3$) has resulted in compounds exhibiting spin transition, as if the Ni(dmit)$_2$ anion increases the cooperativity within the

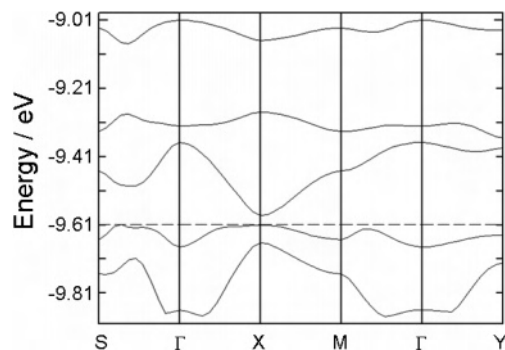(47) Ren, J.; Liang, W.; Whangbo, M.-H. *Crystal and Electronic Structure Analysis Using CAESAR.* http://www.primeC.com. 1998.

Figure 16. Electronic band structure calculated with the EHTB method for the five LUMO bands of the [Ni(dmit)$_2$] slab, with the projections in the reciprocal lattice S(−1/2,1/2), Γ(0,0), X(1/2,0), Y(0,1/2) and M(1/2,1/2).

compound, as a result of its tendency to form layers and consequently to force the iron counterions to lie close to each other. **3** has been obtained directly as a fractional oxidation state complex. It exhibits a gradual and broad spin transition between 350 and 100 K, together with a semiconducting behavior. It is the second molecular compound exhibiting both properties, after [Fe(qsal)$_2$][Ni(dmit)$_2$]$_3$·CH$_3$CN·H$_2$O reported by Takahashi et al.[25] Despite these features, work is still needed to understand the non-ohmic nature of **3** below 100 K and to correlate it with the magnetic properties.

Supporting Information Available: Table of short intermolecular contacts in **1** and figures of the projection and the electronic band structure of of **3**. This material is available free of charge via the Internet at http://pubs.acs.org.

IC062461C